WHOI-81-21
Copy 1

Woods Hole Oceanographic Institution
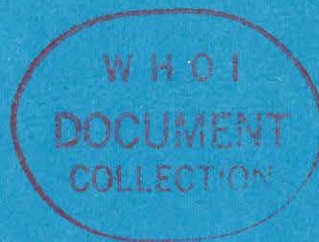
WOODS HOLE OCEANOGRAPHIC INSTITUTION

1930

THE CONTRIBUTION OF NORMAL MODES IN THE
BOTTOM TO THE ACOUSTIC FIELD IN THE OCEAN

by

Mark K. Macpherson
and
George V. Frisk

April 1981

TECHNICAL REPORT

WOODS HOLE, MASSACHUSETTS 02543

WHOI-81-21

THE CONTRIBUTION OF NORMAL MODES IN THE BOTTOM TO THE ACOUSTIC FIELD IN THE OCEAN

by

Mark K. Macpherson
and
George V. Frisk

WOODS HOLE OCEANOGRAPHIC INSTITUTION
Woods Hole, Massachusetts 02543

April 1981

TECHNICAL REPORT

Approved for Distribution: Earl E. Hays, Chairman
                          Department of Ocean Engineering

The contribution of normal modes in the bottom to the acoustic field in the ocean

Mark K. Macpherson[a] and George V. Frisk

Woods Hole Oceanographic Institution, Woods Hole, Massachusetts 02543

The effects of normal modes in the bottom on the acoustic field in the ocean are examined. The ocean bottom model consists of a slow isovelocity layer overlying an isovelocity half-space to simulate the characteristic sound velocity drop at the water–bottom interface. Attention is focused on the perfectly trapped modes which are excited in the layer by inhomogeneous waves emitted by a point source in the water column. The relative normal mode contribution to the total acoustic field in the water is calculated analytically for a near-bottom source/receiver geometry and evaluated for representative ocean bottom examples. It is shown that, for combined source/receiver heights less than a wavelength, the field is dominated by the leaky mode contribution at short ranges ($\lesssim 2$ km) and the trapped mode contribution at long ranges ($\gtrsim 2$ km). For fixed bottom parameters, the trapped mode contribution increases exponentially with decreasing combined source/receiver height. It is also shown that, for a fixed layer wavenumber–thickness product and fixed layer sound speed, the leaky mode fields at different frequencies are approximately range-scaled versions of the same field.

INTRODUCTION

It has been shown[1,2] that deep-sea sediments characteristically exhibit a lower sound speed in the upper few meters than in the immediate overlying ocean. This low speed layer can be expected to support acoustic energy in the form of normal modes that will alter the sound field in the deep ocean. The trapping of energy in the sediment from the ocean would proceed by a coupling process that was proposed by Lamb[3] and was extended for geophysical cases by Press and Ewing[4] and Jardetzky and Press.[5] Analogous problems exist within the water column in the form of surface ducts and have been investigated by Labianca[6] and others.[7,8] Theoretical considerations of propagation in slab configurations have been made by Tamir and Felsen[9] and Fiorito and Überall,[10] for example.

In particular, perfectly trapped normal modes can be excited in the low speed layer by a source in the water column because the source emits an angular spectrum of plane waves[11] which includes waves at complex angles of incidence $\theta = \pi/2 - i\alpha$ ($\alpha > 0$). The source couples into the trapped modes via these exponentially decaying inhomogeneous waves. These modes manifest themselves as resonances (arising from poles) in the plane wave reflection coefficient for the layer.[12] By determining the strength of these modes in the water column, it will be possible to assess the feasibility of measuring these resonances.[13–17]

In this paper we examine the contribution of these trapped modes to the total acoustic field when the bottom consists of a slow isovelocity fluid layer overlying an isovelocity fluid half-space. The water is modeled as an isovelocity half-space, and therefore the effects of gradients and surface reflections are neglected. For simplicity, the effects of attenuation have not been included in this model. The theory is based on the me-

thod used by Ewing, Jardetzky, and Press[18] (EJP) for the two-fluid half-space problem. It requires that the horizontal range between source and receiver be much greater than both the wavelength and the combined source/receiver height. This near-bottom geometry is suitable to our case since we expect the effect of the trapped modes to be greatest in the vicinity of the water–bottom interface. It is to be contrasted with the approach of Brekhovskikh,[11] for example, who requires that the source/receiver height be much greater than the wavelength.

Using the EJP method, we can decompose the total field into the following elements: (a) incident wave, (b) specularly reflected wave at the upper interface, (c) lateral (refracted) wave at the lower interface, (d) perfectly trapped normal modes, (e) modes which are leaky at the upper interface only, and (f) modes which are leaky at both interfaces. We shall investigate the relative contributions of these various elements as a function of source/receiver height, frequency, layer thickness, and sound velocity within the layer.

I. THEORY

For a spherical wave of amplitude p_0 emitted by a point source located in isovelocity water overlying a horizontally stratified bottom, Fourier decomposition into an effective infinite sum of plane waves gives the solution for the excess acoustic pressure in the form[11,18]

$$p(r,z) = p_0 \int_0^\infty \frac{e^{-\kappa_0|z-z_0|}}{\kappa_0} J_0(k_r r) k_r \, dk_r$$

$$+ p_0 \int_0^\infty R(k_r) \frac{e^{-\kappa_0(z+z_0)}}{\kappa_0} J_0(k_r r) k_r \, dk_r. \quad (1)$$

The point source (of angular frequency ω) and receiver are separated by a range r and are located at heights z_0 and z above the interface, respectively. J_0 is the zero-order Bessel function and $R(k_r)$ is the plane wave

reflection coefficient and is, in general, a function of frequency and horizontal wavenumber k_r. κ_0 is the vertical wavenumber in the water and is given by

$$\kappa_0 = (k_r^2 - k_0^2)^{1/2}, \qquad (2)$$

where $k_0 = \omega/c_0$ is the water wavenumber and c_0 is the water sound speed. A time dependence of $e^{-i\omega t}$ has been suppressed.

The sound-speed profile and source/receiver geometry for the model under investigation are shown in Fig. 1. As is seen from the figure, this model has three layers. Isovelocity water (with density ρ_0 and sound speed c_0) overlies a sediment layer (ρ_1, c_1) with a lower sound speed, below which is a high velocity fluid half-space (ρ_2, c_2). This model is an approximation to a realistic profile[2] in that the sediment layer could be expected to show a positive sound speed gradient, as shown in Fig. 2. However, the model of Fig. 1 greatly simplifies the analysis and will be the subject of investigation in this paper.

The reflection coefficient for the model of Fig. 1 is given by[11]

$$R(k_r) = \frac{R_{01}(k_r) + R_{12}(k_r)e^{2\kappa_1 H}}{1 + R_{01}(k_r)R_{12}(k_r)e^{2\kappa_1 H}}, \qquad (3a)$$

where

$$R_{01}(k_r) = (m_1\kappa_0 - \kappa_1)/(m_1\kappa_0 + \kappa_1) \qquad (3b)$$

and

$$R_{12}(k_r) = (m_2\kappa_1 - \kappa_2)/(m_2\kappa_1 + \kappa_2) \qquad (3c)$$

are the Rayleigh reflection coefficients for sound incident on the water-sediment interface and the sediment-basement interface, respectively. Here $m_1 = \rho_1/\rho_0$, $m_2 = \rho_2/\rho_1$, and κ_1 and κ_2 are the vertical wavenumbers in media 1 and 2, respectively (cf. Fig. 1).

The solution for the acoustic pressure given by Eq. (1) can be found by the methods of complex analysis. In the following, a method similar to that used by EJP[18] for the two-fluid half-space problem is followed.

First, the two integrals of Eq. (1) are combined to give

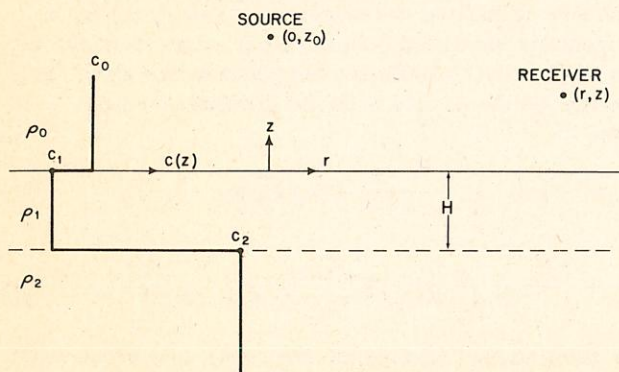$$p(r,z) = 2p_0 \int_0^\infty \Lambda(k_r) J_0(k_r r) k_r \, dk_r, \qquad (4a)$$

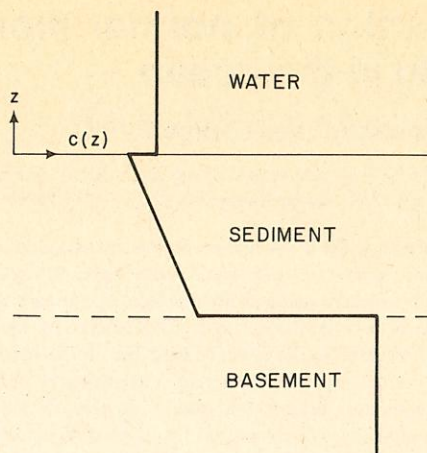FIG. 1. Geometry and sound speed profile for the slow speed layer model.

FIG. 2. Characteristic water-bottom sound speed profile.

where (for $z < z_0$)

$$\Lambda(k_r) = (m_1\kappa_0 + \kappa_1)^{-1}(e^{-\kappa_0 z_0}/\kappa_0)$$
$$\times [m_1\kappa_0 \cosh\kappa_0 z + \kappa_1 \sinh\kappa_0 z + R_{12}e^{2\kappa_1 H}(m_1\kappa_0 \cosh\kappa_0 z$$
$$- \kappa_1 \sinh\kappa_0 z)]/D(k_r) \qquad (4b)$$

and $D(k_r)$ is the denominator of the reflection coefficient $R(k_r)$ of Eq. (3a). A similar expression for $\Lambda(k_r)$ may be obtained for $z > z_0$ by interchanging z and z_0.

The substitution of

$$2J_0(k_r r) = H_0^{(1)}(k_r r) + H_0^{(2)}(k_r r) \qquad (5)$$

is made in Eq. (4a), which gives $p(r,z)$ as the sum of two integrals

$$p(r,z) = p_0 \int_0^\infty \Lambda(k_r)H_0^{(1)}(k_r r)k_r \, dk_r$$
$$+ p_0 \int_0^\infty \Lambda(k_r)H_0^{(2)}(k_r r)k_r \, dk_r. \qquad (6)$$

In evaluating the two integrals of Eq. (6), we replace k_r by the complex variable $\zeta = k_r + i\tau$. Both integrations of Eq. (6) are along the real axis in the complex ζ plane. However, it is advantageous to extend them into closed loops. This extension is illustrated in Fig. 3. The first integral is extended to enclose the first quadrant by adding the contributions of the positive imaginary axis and the infinite arc joining the points $+\infty$ and $+i\infty$. Similarly, the second integral is extended into the fourth quadrant by adding the negative imaginary axis and the infinite arc joining the points $+\infty$ and $-i\infty$.

This method is helpful in that the integrals around these closed loops can be expressed in terms of a residue series of any pole singularities and branch line integrals arising from branch point singularities in the first and fourth quadrants. It is to be noted however, that the integrations along the positive and negative imaginary axes and the infinite arcs need to be evaluated before the solution of Eq. (6) can be found. These latter integrations can be evaluated quite simply.

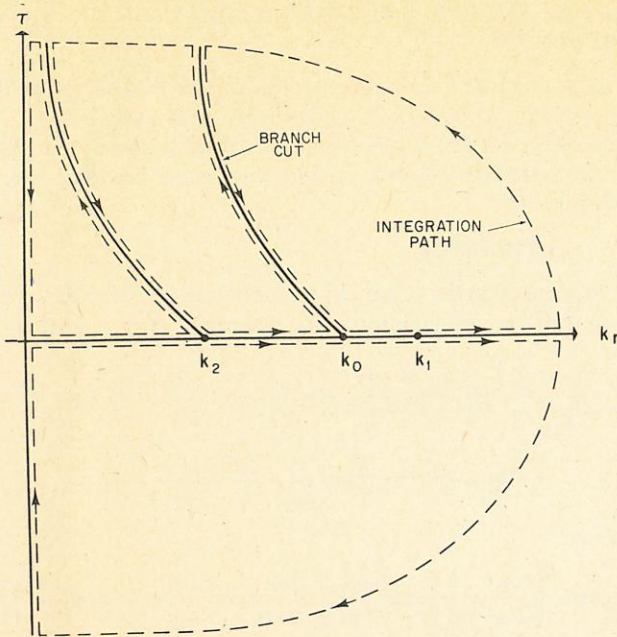By inspection of the asymptotic forms for $H_0^{(1)}$ and

FIG. 3. Paths of integration in the complex ζ plane.

$H_0^{(2)}$,[19] it is seen that they vanish along the infinite arcs in the first and fourth quadrants respectively. Hence, the integrations along these infinite arcs will also vanish.

Since $H_0^{(1)}(i\tau r) = -H_0^{(2)}(-i\tau r)$ [19] and $\Lambda(\zeta)$ uses the same values of $\kappa_0, \kappa_1, \kappa_2$ on the positive and negative parts of the imaginary axis, the integrations along these two segments cancel.

Hence, the acoustic pressure $p(r,z)$ is represented solely by singularities in the first and fourth quadrants of the complex ζ plane. Thus, we may write

$$p(r,z) = p_1(r,z) + p_2(r,z),\qquad(7)$$

where $p_1(r,z)$ represents the contributions at the branch points and $p_2(r,z)$ the pole contributions.

Both types of singularities arise in the model under consideration and they will be discussed separately.

A. Branch points

Branch point singularities arise from multi-valued functions in the integrand and, in our case, they are introduced by the radicals κ_0 and κ_2. A branch point does not arise due to the radical κ_1 because $\Lambda(\zeta)$ is an even function of κ_1 [cf. Eq. (4b)]. Since κ_2 has a form similar to κ_0 in Eq. (2), the branch points in the complex plane are located at the real positions $(\pm k_0, 0)$ and $(\pm k_2, 0)$ (cf. Fig. 3). These branch points require that the complex ζ plane be divided into four Riemann sheets depending upon the two choices of sign for each of the two radicals. From physical considerations at $z = \infty$ (the radiation condition), it is required that the real parts of each radical be positive. Hence, a particular Riemann sheet is chosen and cuts are made in the complex plane along the lines $\text{Re}(\kappa_0) = 0$, and $\text{Re}(\kappa_2) = 0$.[20]

To make the integrand a uniform function, the closed loop integrations proceed around the borders of those cuts. These branch cuts are illustrated in Fig. 3.

Since the branch cuts are all in the first quadrant, we have

$$p_1(r,z) = p_0 \int_{L_0} \Lambda(\zeta) H_0^{(1)}(\zeta r)\zeta\, d\zeta$$

$$+ p_0 \int_{L_2} \Lambda(\zeta) H_0^{(1)}(\zeta r)\zeta\, d\zeta \qquad(8)$$

where L_0 and L_2 signify integrations over the $\text{Re}(\kappa_0) = 0$ and $\text{Re}(\kappa_2) = 0$ cuts, respectively.

B. L_0 contribution

Using a method similar to that of EJP,[18] the L_0 branch line integral may be evaluated as follows. First, since the contour of integration lies close to the branch cut [given by $\text{Re}(\kappa_0) = 0$], for points on the contour we may write

$$\kappa_0 = \pm i\mu, \quad \zeta^2 = k_0^2 - \mu^2, \qquad(9)$$

and

$$\zeta\, d\zeta = -\mu\, d\mu,$$

where μ is real and varies from 0 to ∞.

The asymptotic form of the Hankel function shows that the major contribution comes from points in the vicinity of the branch point. Physically, this corresponds to the situation where the source and receiver heights above the bottom are small in comparison with their range separation. Hence, in terms of acoustic rays, it is required that the angle of incidence be close to 90° (i.e., grazing incidence). To calculate the contribution for angles not near grazing, a saddle-point method must be used to calculate the branch line integral.[21] This case will not be considered here.

Hence, we may consider μ small and make the following approximations when ζr is large

$$\zeta \approx k_0 - \mu^2/(2k_0),$$
$$\kappa_1 \approx i[\omega/\gamma_{10} + \gamma_{10}\mu^2/(2\omega)], \qquad(10)$$
$$\kappa_2 \approx \omega/\gamma_{02},$$

where

$$\gamma_{10} = (1/c_1^2 - 1/c_0^2)^{-1/2},$$

and

$$\gamma_{02} = (1/c_0^2 - 1/c_2^2)^{-1/2}.$$

If only the first term in the asymptotic expansion of the Hankel function is used, the L_0 integral is given by

$$\int_{L_0} = p_0 \int_0^\infty \left(\frac{2}{\pi k_0 r}\right)^{1/2} \exp\left[i\left(k_0 r - \frac{\pi}{4}\right)\right] [\Lambda(i\mu) - \Lambda(-i\mu)]$$

$$\times \exp[-ir\mu^2/(2k_0)]\mu\, d\mu, \qquad(11a)$$

where on the contour L_0

$$\Lambda(i\mu) - \Lambda(-i\mu)$$

$$= \frac{\cos\mu(z-z_0)}{i\mu} - \frac{\cos\mu(z+z_0)}{i\mu}$$

$$- \frac{2m_1\sin\mu(z+z_0)}{\bar{\kappa}_1}\left(\frac{1-R_{12}^2 e^{4i\bar{\kappa}_1 H}}{(1-R_{12}e^{2i\bar{\kappa}_1 H})^2}\right)$$

$$+ \frac{im_1^2\mu(1+R_{12}e^{2i\bar{\kappa}_1 H})^2}{\bar{\kappa}_1^2(1-R_{12}e^{2i\bar{\kappa}_1 H})^2}\left[\cos\mu(z-z_0)+\cos\mu(z+z_0)\right], \tag{11b}$$

where $\bar{\kappa}_1 = (k_1^2 - k_r^2)^{1/2}$ and we assume positive square roots throughout.

The four integrals of Eq. (11a), implied from Eq. (11b), can be found from a table of integrals[22] and the results are (with R_{12} evaluated at $k_r = k_0$).

$$\int_{L_0}^{(\text{I})} = \frac{p_0}{r}\exp\left[ik_0\left(r+\frac{(z-z_0)^2}{2r}\right)\right], \tag{12a}$$

$$\int_{L_0}^{(\text{II})} = -\frac{p_0}{r}\exp\left[ik_0\left(r+\frac{(z+z_0)^2}{2r}\right)\right], \tag{12b}$$

$$\int_{L_0}^{(\text{III})} = p_0\frac{2m_1\gamma_{10}}{c_0 r^2}\left[\frac{1-R_{12}^2 e^{4i\omega H \hbar_{10}}}{(1-R_{12}e^{2i\omega H \hbar_{10}})^2}\right](z+z_0)$$

$$\times \exp\left[ik_0\left(r+\frac{(z+z_0)^2}{2r}\right)\right], \tag{12c}$$

$$\int_{L_0}^{(\text{IV})} = -p_0\frac{m_1^2 i\gamma_{10}}{c_0 r^2}\left(\frac{(1+R_{12}e^{2i\omega H \hbar_{10}})^2}{(1-R_{12}e^{2i\omega H \hbar_{10}})^2}\right)$$

$$\times \left\{\left(\frac{1}{\omega}-\frac{i(z+z_0)^2}{c_0 r}\right)\exp\left[ik_0\left(r+\frac{(z+z_0)^2}{2r}\right)\right]\right.$$

$$\left.+\left(\frac{1}{\omega}-\frac{i(z-z_0)^2}{c_0 r}\right)\exp\left[ik_0\left(r+\frac{(z-z_0)^2}{2r}\right)\right]\right\}. \tag{12d}$$

Physically, Eq. (12a) represents the direct spherical wave traveling from source to receiver for small $(z-z_0)/r$, while Eq. (12b) corresponds to the grazing reflection from the interface at the specular angle $\theta_0 = \tan^{-1}[r/(z+z_0)]$ for small $(z+z_0)/r$. A schematic of these arrivals is given in Fig. 4. The reflected wave is 180° out of phase with the direct wave due to the fact that the plane wave reflection coefficient approaches -1 in the limit of grazing incidence. The superposition
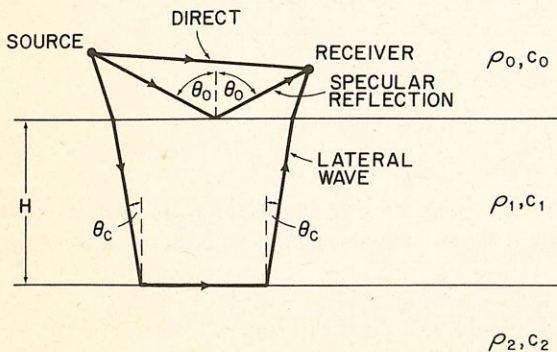

FIG. 4. The direct, specularly reflected, and lateral wave arrivals.

of Eqs. (12a) and (12b) therefore leads to the Lloyd mirror effect.[23]

It is seen that Eqs. (12c) and (12d) are dependent on the properties of both media and decay with range as r^{-2}. These terms are higher-order contributions to the specular field and arise from the curvature of the incident wavefront.[24]

C. L_2 contribution

The calculation of the L_2 branch-line integral proceeds in a similar manner to the L_0 integral. The result is

$$\int_{L_2} = \left\{-2i\left(\frac{m_1}{m_2}\right)p_0\bigg/\left[c_2 r^2 \omega\left(\frac{m_1^2}{\gamma_{02}^2}\cos^2\frac{\omega H}{\gamma_{12}}+\frac{1}{\gamma_{12}^2}\sin^2\frac{\omega H}{\gamma_{12}}\right)\right]\right\}$$

$$\times \exp(-2i\Phi)\exp\left[i\omega\left(\frac{r}{c_2}+\frac{2H}{\gamma_{12}}-\frac{(z+z_0)}{\gamma_{02}}\right)\right], \tag{13a}$$

where

$$\Phi = \tan^{-1}\left\{\left(\frac{m_1}{\gamma_{02}}-\frac{1}{\gamma_{12}}\right)\sin\frac{2\omega H}{\gamma_{12}}\bigg/\left[2\left(\frac{m_1}{\gamma_{02}}\cos^2\frac{\omega H}{\gamma_{12}}+\frac{1}{\gamma_{12}}\sin^2\frac{\omega H}{\gamma_{12}}\right)\right]\right\}, \tag{13b}$$

and

$$\gamma_{02} = (1/c_0^2 - 1/c_2^2)^{-1/2}, \tag{13c}$$

$$\gamma_{12} = (1/c_1^2 - 1/c_2^2)^{-1/2}.$$

This term is dependent on the properties of all three media and is seen to decrease with range as r^{-2}. An examination of the phases in Eq. (13) shows that the path of propagation is that of the lateral (refracted) wave, where acoustic energy couples into the sediment-lower half-space boundary at the critical angle $\theta_c = \sin^{-1}(c_1/c_2)$, travels along the interface, and re-radiates into the overlying sediment layer and water at the same angle. The effects of the lateral wave are well-known[25] and will not be discussed in detail here. A schematic of the lateral wave arrival is given in Fig. 4.

D. Poles

The pole contributions can be expressed simply in terms of a standard residue series. From physical considerations of attenuation it is well-known that all poles lie in the first quadrant.[26] If, initially, poles lie along the real axis, an introduction of small losses will shift them slightly into the first quadrant.

We therefore have

$$p_2(r,z) = 2\pi i p_0 \sum_n H_0^{(1)}(\xi_n r)\xi_n N(\xi_n)\left(\frac{\partial D(\xi_n)}{\partial \xi_n}\right)^{-1}, \tag{14a}$$

where [from Eqs. (3) and (4)] for $z < z_0$

$$N(\zeta) = (m_1\kappa_0+\kappa_1)^{-1}\frac{e^{-\kappa_0 z_0}}{\kappa_0}[m_1\kappa_0\cosh\kappa_0 z + \kappa_1\sinh\kappa_0 z$$

$$+ R_{12}(\zeta)e^{2i\kappa_1 H}(m_1\kappa_0\cosh\kappa_0 z - \kappa_1\sinh\kappa_0 z)], \tag{14b}$$

and

$$D(\zeta) = 1 + R_{01}(\zeta)R_{12}(\zeta)e^{2i\kappa_1 H}. \tag{14c}$$

Each pole is represented by a particular value of n and it is assumed in Eqs. (14b) and (14c) that each subscrip-

ted κ is dependent upon n.

The differentiation of Eq. (14c) can be performed and the contribution of the poles to the acoustic pressure be found. However, the actual solution is dependent upon the positions of the poles in the complex ζ plane. There are three distinct types of poles, each of which has a different physical interpretation.

Figure 5 is a schematic plot of the pole positions in the ζ plane for the model of Fig. 1. The sequence of wavenumbers is as shown since the highest sound speed is in the lower half-space and the lowest sound speed is in the sediment layer.

In the region of horizontal wavenumbers greater than the water wavenumber k_0 but less than the sediment wavenumber k_1, the poles lie on the real axis. In terms of acoustic rays, these poles correspond to plane waves trapped inside the low-speed sediment layer by repeated total reflections at both interfaces. They may also be interpreted as acoustic normal modes[27] propagating radially in the sediment, with the characteristic sinusoidal depth dependence within the layer and the exponential decay away from the interfaces in both the lower half-space and water.

The residue series for these trapped normal modes is found to be

$$p_2^{(T)}(r,z) = -2\pi i \rho_0 \sum_n H_0^{(1)}(k_r r) e^{-\bar{\kappa}_0(z+z_0)}\left(\frac{m_1 \bar{\kappa}_1^2}{m_1^2 \bar{\kappa}_0^2 + \bar{\kappa}_1^2}\right)$$
$$\times \left(H - \frac{m_1(\bar{\kappa}_0^2 + \bar{\kappa}_1^2)}{\bar{\kappa}_0(m_1^2 \bar{\kappa}_0^2 + \bar{\kappa}_1^2)} - \frac{m_2(\bar{\kappa}_2^2 + \bar{\kappa}_1^2)}{\bar{\kappa}_2(m_2^2 \bar{\kappa}_1^2 + \bar{\kappa}_2^2)}\right)^{-1},$$

(15a)

where

$$\bar{\kappa}_0 = (k_r^2 - k_0^2)^{1/2},$$
$$\bar{\kappa}_1 = (k_1^2 - k_r^2)^{1/2}, \qquad (15b)$$
$$\bar{\kappa}_2 = (k_r^2 - k_2^2)^{1/2},$$

are the vertical wavenumbers in the three media.

The positions of these poles can be calculated approximately by use of a method similar to that of Brekhovskikh.[28] For reflections beyond the critical angle, the Rayleigh reflection coefficients R_{10} and R_{12} may each be written with unit magnitude and phases $2\psi_{10}$ and $2\psi_{12}$, respectively. These phases are given by

$$\psi_{12} = -\tan^{-1}[b_2 \rho_1 c_1 / (\rho_2 c_2 \cos\theta_1)], \qquad (16)$$

τ

k_2 k_0 k_1 k_r
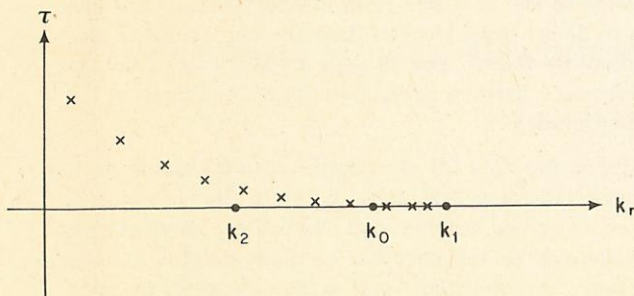
FIG. 5. Schematic illustration of pole positions in the complex ζ plane.

where

$$b_2 = [(c_2/c_1)^2 \sin^2\theta_1 - 1]^{1/2},$$

and θ_1 is the angle of incidence to the sediment–lower half-space interface and $k_r = k_1 \sin\theta_1$. Phase ψ_{10} is similar, with c_0, ρ_0 replacing c_2, ρ_2. Hence, the defining equation for the pole positions can be written as

$$\exp[2i(\psi_{10} + \psi_{12} + \kappa_1 H)] = 1. \qquad (17)$$

This is true when

$$\kappa_1 H = (n-1)\pi - \psi_{10} - \psi_{12} \quad (n=1,2,3,\ldots). \qquad (18)$$

Phases ψ_{10} and ψ_{12} may be calculated by assuming a first approximation of perfect reflection in Eq. (18) (i.e., $\psi_{10}, \psi_{12} = \pi/2$). A value for θ_1 is found for this approximation and Eq. (16) is used to calculate ψ_{12} (similarly for ψ_{10}). These results are resubstituted in Eq. (18) to find the eigenvalues κ_1.

In the wavenumber region less than the water wavenumber k_0 but greater than the lower half-space wavenumber k_2, the pole positions have significant imaginary parts. In a ray description they correspond to plane waves totally reflected at the sediment–lower half-space interface but partially transmitted into the overlying water. Hence, energy is continually lost from the sediment waveguide. In the normal mode representation these waves are termed "leaky" modes.[29]

The expression for the acoustic pressure of these modes is

$$p_2^{(L)}(r,z) = 2\pi i \rho_0 \sum_n H_0^{(1)}(\zeta r) e^{i\bar{\kappa}_0(z+z_0)}\left(\frac{2m_1 \bar{\kappa}_1^2}{(m_1^2 \bar{\kappa}_0^2 - \bar{\kappa}_1^2)}\right)$$
$$\times \left(H + \frac{im_1(\bar{\kappa}_0^2 - \bar{\kappa}_1^2)}{\bar{\kappa}_0(m_1^2 \bar{\kappa}_0^2 - \bar{\kappa}_1^2)} - \frac{m_2(\bar{\kappa}_2^2 + \bar{\kappa}_1^2)}{\bar{\kappa}_2(m_2^2 \bar{\kappa}_1^2 + \bar{\kappa}_2^2)}\right)^{-1},$$

(19a)

where

$$\bar{\kappa}_0 = (k_0^2 - \zeta^2)^{1/2},$$
$$\bar{\kappa}_1 = (k_1^2 - \zeta^2)^{1/2}, \qquad (19b)$$
$$\bar{\kappa}_2 = (\zeta^2 - k_2^2)^{1/2}.$$

The pole positions may be found from Eq. (18) with the real part of $\psi_{10} = 0$ (since the angle of incidence is less than critical) and the imaginary part given by[28]

$$-\tfrac{1}{2}\ln[-R_{10}(k_r)].$$

Hence, the pole positions are found from

$$\kappa_1 H = [(n - \tfrac{1}{2})\pi - \psi_{12}] + \frac{i}{2}\ln(R_{10}) \quad (n=1,2,3,\ldots). \qquad (20)$$

For horizontal wavenumbers less than k_2 there is partial transmission at each reflection with acoustic energy leaking out of the waveguide into both the water and basement. The pole positions may be found using Eq. (20) in a manner similar to that described above, with the appropriate substitution for ψ_{12}. These waves are also termed "leaky" modes and are given by an expression similar to Eq. (19). In the following section these leaky modes are referred to as type II, while those given by Eq. (19) are termed type I.

All three types of waves arising from poles can be

excited by a source located outside the sediment layer.[30] Leaky modes are excited from the partial transmission of acoustic waves incident upon the water-sediment interface. The characteristic modal standing wave pattern is set up by the interference of up- and down-going plane waves within the layer. Attenuation with range is introduced by partial reflections at the interfaces.

The physical process involved in exciting the trapped normal modes is not as straightforward since, if a ray model is assumed, there are no ray paths which enter the waveguide. However, there is a diffracted field in the water propagating parallel to the water-sediment interface and exponentially decaying away from it. A point source emits a spectrum of plane waves which includes these "inhomogeneous waves"[31] at complex angles $\pi/2 - i\alpha (\alpha > 0)$ in addition to those at real angles. The source therefore provides a mechanism for exciting the perfectly trapped modes by coupling into them via the inhomogeneous wave field.[12]

II. RESULTS

In this section, the relative importance of the trapped modes to the acoustic field in the water close to the ocean bottom will be discussed. The effects of the combined source/receiver height, sediment sound channel thickness, source frequency, and sound speed within the layer on these trapped modes will be investigated.

An attempt has been made here to choose physical parameters which are representative of the real ocean. The work of Hamilton[1,2] has shown that there are generally positive sound speed gradients in the sea floor with the surficial deep-sea sediments exhibiting a lower sound speed than the immediate overlying water mass. This sediment sound speed has been found to be as much as 3% lower than the water sound speed. With gradients from 0.5 s^{-1} to 1.5 s^{-1} in the sediment, one expects sound channel heights to vary from 5 to 95 m.[1]

In the following, the sound speeds in the water and lower half-space were chosen as 1540 and 1700 m/s, respectively, and densities of 1.0 g/cm^3, 1.5 g/cm^3, and 2.0 g/cm^3 were assigned to the water, sediment channel, and lower half-space, respectively. These values are unchanged throughout this section.

A. Dependence on source/receiver heights

Figure 6(a) presents propagation loss (dB) versus range for a progressive coherent addition of the separate elements of the acoustic field.[32] The source frequency is 110 Hz, there is a 3% decrease in sound speed at the water-sediment interface, and the sediment sound channel is 90 m thick. The source and receiver are each 10 m above the sea bottom and the combined source/receiver height is given as a fraction of the acoustic wavelength in the water (λ_0 = water sound speed/source frequency) in the figure caption. In each plot, zero dB is taken as the level of the total acoustic field at a range of 100 m from the source. Therefore absolute comparisons between different plots should

not be made. The plots do not include closer ranges since in this region the assumption of large horizontal ranges in comparison with the combined source/receiver height is no longer valid. Because of this choice of the zero dB level, interference effects may make it possible for the acoustic field at ranges slightly greater than 100 m to be higher than zero dB. This is evident in some of the figures.

The lowest curve of Fig. 6(a) is the relative propagation loss of the trapped modes alone and exhibits a characteristic modal interference pattern for the three propagating modes of this example.

The trapped modes plus specular curve, as labeled in the figure, decay as r^{-2}. This is expected from the Lloyd mirror effect when both source and receiver are located close to the interface. There is little or no interference evident in the curve since the level of the trapped modes is far below that of the specular field. However, an interference pattern is apparent in the trapped modes plus specular plus lateral wave curve. This occurs since the lateral wave and specular field both decay with range as r^{-2}.

The curve of the total acoustic field is at a higher level for short ranges because of the large contribution of the ten propagating leaky modes. However, at a range of approximately 2 km the leaky mode field has decayed sufficiently to leave the total acoustic field as the interference pattern of the specular field and lateral wave. As mentioned earlier, the large range dependent losses of these leaky modes are due to imperfect reflections at the water-sediment interface and also (for type II) at the sediment-lower half-space interface.

Figure 6(b) presents results with the same physical parameters as Fig. 6(a) with the exception that both the source and receiver heights are 5 m. Hence, the number of trapped and leaky modes are the same as in Fig. 6(a). In this and all ensuing plots in this section, the source and receiver heights are equal (i.e., $z = z_0$). It is obvious from the figure that the relative level of the trapped modes is higher with the source and receiver closer to the water-sediment interface. This indicates that the relative strength of the trapped modes to the acoustic field is dependent on the source and receiver height. Interference patterns set up by the trapped modes and specular field and also by the trapped modes, specular, and lateral wave are evident in the figure. The leaky modes make a large contribution to the acoustic field at short ranges but are seen to decay quickly until they are negligible at approximately 2 km. For ranges greater than 2 km the interference pattern oscillates about the curve of the trapped modes.

Figures 6(c) and (d) are graphs with the same physical parameters as Fig. 6(a), but with the combined source/receiver heights at 2 and 0.2 m, respectively. With the source and receiver at these heights above the interface, the specular field makes a negligible contribution. There is slight interference between the trapped modes and lateral wave evident in the figures

for short ranges. The major contribution at short ranges is due to the leaky modes. However, this term decays to effectively zero at 1.5 km in both figures and the contributing term at greater ranges is due to the trapped modes.

It is evident from Fig. 6 that the relative strength of the trapped modes progressively increases as the combined source and receiver heights decrease. This can be explained in an analytic manner as follows.

From Eq. (15) the acoustic pressure due to these trapped modes can be written in the form

$$p_2^{(T)}(k_{r_n}, z, z_0) = \sum_{n=1}^{N} A_n \exp[-(k_{r_n}^2 - k_0^2)^{1/2}(z + z_0)], \quad (21)$$

where A_n may be found from Eq. (15) and is frequency dependent.

Equation (21) may be rewritten as

$$p_2^{(T)}(k_{r_n}, z, z_0)$$
$$= \exp[-(k_{r_1}^2 - k_0^2)^{1/2}(z + z_0)]$$
$$\times (A_1 + A_2 \exp\{[(k_{r_1}^2 - k_0^2)^{1/2} - (k_{r_2}^2 - k_0^2)^{1/2}](z + z_0)\}$$
$$+ \cdots + A_N \exp\{[(k_{r_1}^2 - k_0^2)^{1/2} - (k_{r_N}^2 - k_0^2)^{1/2}](z + z_0)\}).$$
$$(22)$$

The exponentials in Eq. (22) may be expanded to give
$$p_2^{(T)}(k_{r_n}, z, z_0)$$

$$= \exp[-(k_{r_1}^2 - k_0^2)^{1/2}(z + z_0)] \left\{ \sum_{n=1}^{N} A_n \right.$$

$$+ (z + z_0) \sum_{n=2}^{N} A_n[(k_{r_1}^2 - k_0^2)^{1/2} - (k_{r_n}^2 - k_0^2)^{1/2}]$$
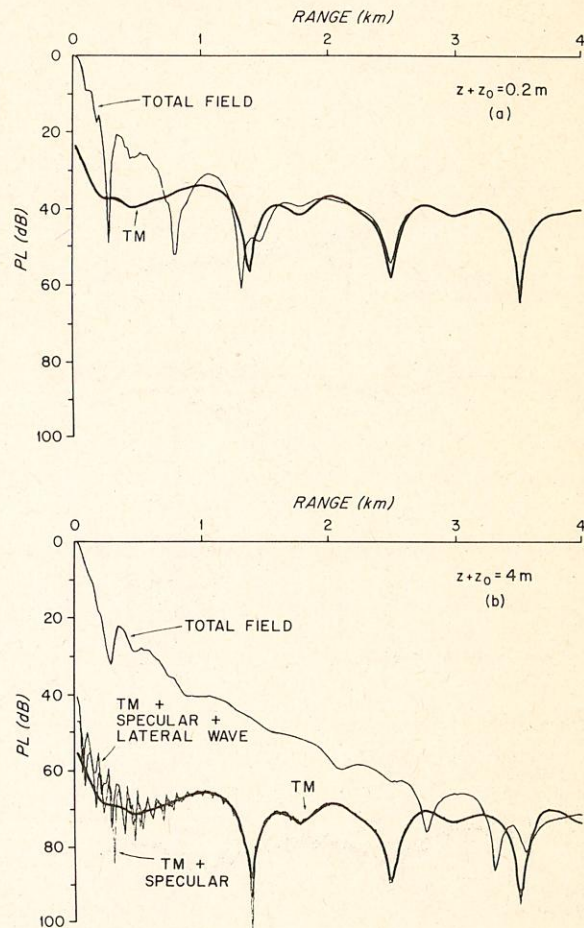
$$\left. + O[(z + z_0)^2] \right\}.$$
$$(23)$$
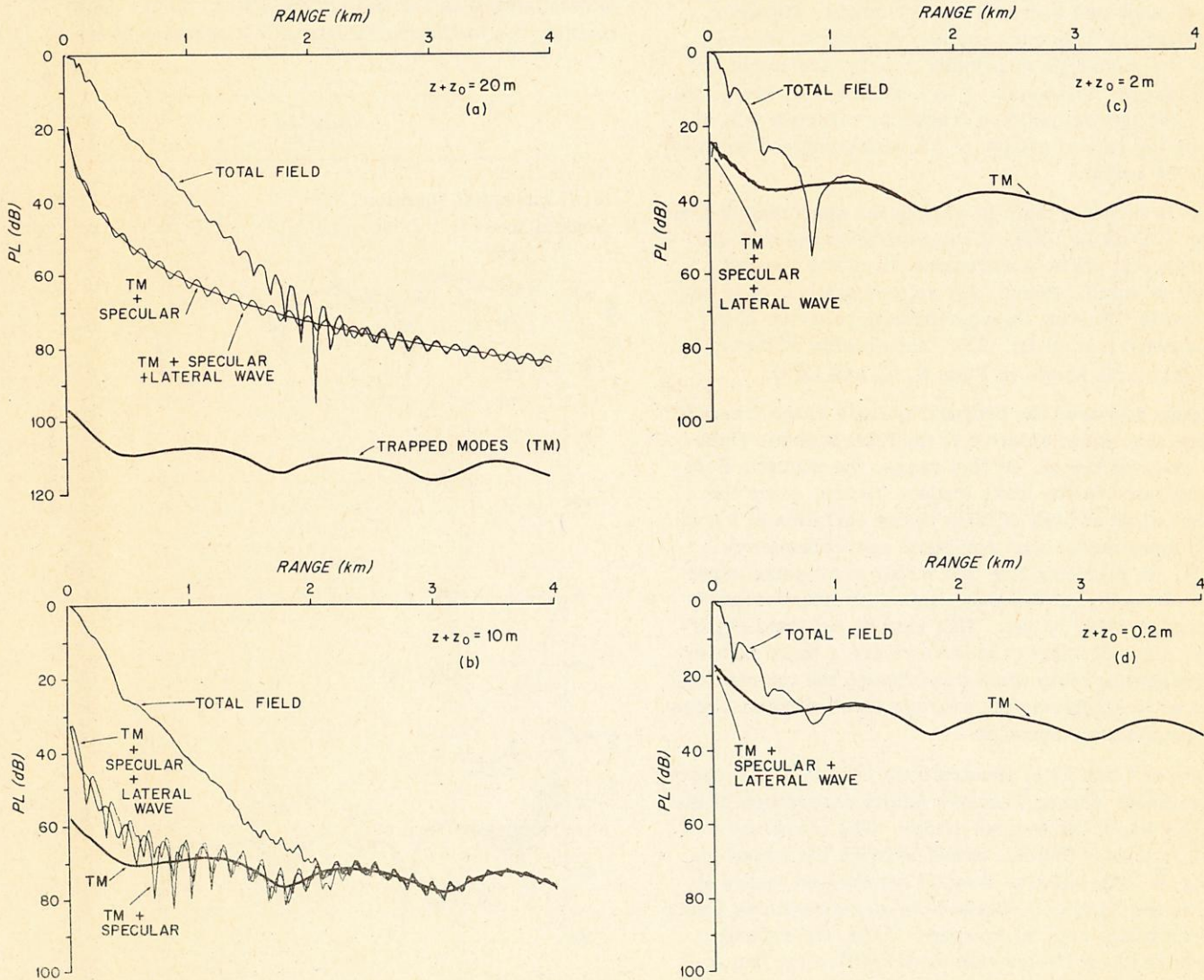
FIG. 6. Propagation loss vs range for $f = 110$ Hz and different source/receiver heights: (a) $(z + z_0)/\lambda_0 = 1.4$, (b) $(z + z_0)/\lambda_0 = 0.7$, (c) $(z + z_0)/\lambda_0 = 0.14$, (d) $(z + z_0)/\lambda_0 = 0.014$. $H = 90$ m, 3% decrease in sound speed. Three trapped modes, ten leaky modes.

Hence, the propagation loss (PL) of the trapped modes is given by

$$PL = -20 \log_{10}(|p_2^{(T)}|/\text{Norm}),$$
$$= 20(\log_{10}e)(k_{r_1}^2 - k_0^2)^{1/2}(z + z_0) \qquad (24)$$
$$- 20\log_{10}\left(\sum_n A_n + \ldots\right) + 20\log_{10}(\text{Norm}),$$

where Norm is the total field normalization constant.

If only the leading order $(z + z_0)$ term in Eq. (24) is retained, then the propagation loss of the trapped modes is expected to be a function of frequency and combined source/receiver height. This is easily seen from Eq. (24), which can be rewritten as

$$PL \approx 20(\log_{10}e)\omega(z + z_0)(1/c_{r_1}^2 - 1/c_0^2)^{1/2}$$
$$- 20\log_{10}\left(\sum_n A_n\right) + 20\log_{10}(\text{Norm}), \qquad (25)$$

where c_{r_1} is the phase velocity of mode one and ω is the angular frequency. From Eq. (25) it is expected that the PL of the trapped modes will be a linear function of combined source/receiver height. However, the effects of frequency are not as straightforward since the modal phase velocity c_{r_1}, A_n, and Norm are all frequency dependent. It is expected, however, that to a first approximation a frequency increase will increase the rate of change of PL with combined source/receiver height.

It is to be noted that, in writing the approximate form of Eq. (24) as Eq. (25), it has been assumed that the difference in vertical wavenumbers of the trapped modes is small. Hence, any representative mode may be used in obtaining the approximate behavior of the propagation loss of Eq. (25). The validity of this approximation is shown in Figs. 6, 7, and 12(a).

Figure 6 showed the propagation loss of the trapped modes, measured relative to the total acoustic field at a range of 100 m. At this range, the acoustic field is dominated by the leaky modes. Hence, since the figures show an approximate linear variation of PL of the trapped modes with combined source/receiver height, we may conclude that within reasonable error the contribution of the leaky modes is independent of source/receiver height. This may be expected physically, since at short ranges there are a large number of propagating leaky modes and though the interference patterns are different the average level of these modes is approximately constant.

Figures 7 and 12(a) illustrate the effects of frequency on the linear source/receiver height dependence of the relative PL of the trapped modes. The frequency in these figures is 220 Hz, which is twice the frequency of Fig. 6. The relative level of the trapped modes is seen in the figures to increase in an approximate linear manner with $z + z_0$, as expected. Also, the rate of change of PL of the trapped modes with $z + z_0$ has increased with the higher frequency of Figs. 7 and 12(a). This result is expected from Eq. (25).

From these plots (and others not included) we con-

clude that the trapped modes can make significant contributions to the acoustic field when the combined source/receiver height is less than a wavelength.

It is to be noted that the relative PL levels for different frequencies, at fixed $z + z_0$, cannot be ascertained from the above results. This occurs since the total acoustic field is also dependent on leaky mode, specular field, and lateral wave contributions which have complex frequency dependencies. These effects are examined in the next section.

B. Dependence on frequency, layer thickness, and sound velocity within the layer

In the previous analysis, we considered situations in which the acoustic properties, and therefore the normal modes, in the bottom remained the same while we varied the source/receiver height in the water. We shall now examine the case where source/receiver height remains constant ($z = z_0 = 1$ m) and we vary the frequency, layer thickness, and sound velocity within the layer. Since these parameters determine the normal modes which are established, there is a complicated effect on the field in the water. In our discussion, we shall concentrate on the behavior of the

FIG. 7. Propagation loss versus range for $f = 220$ Hz and different source/receiver heights: (a) $(z + z_0)/\lambda_0 = 0.029$, (b) $(z + z_0)/\lambda_0 = 0.57$. $H = 90$ m, 3% decrease in sound speed. Six trapped modes, 20 leaky modes. See also Fig. 12(a).

normal modes (both leaky and trapped) since they again make the dominant contribution to the total field.

The normal modes which are excited in a particular case depend upon the corresponding pole positions in the complex ζ plane. From Eqs. (3), (16), (18), and (20) we can infer that the dimensionless pole positions $\zeta' = \zeta/k_1$ are functions of the density ratios m_1 and m_2, the dimensionless wavenumbers k_2/k_1 and k_0/k_1, and the parameter k_1H. We will first examine the effect on the pole locations of varying k_1H while keeping the remaining parameters fixed. In Fig. 8 the pole positions are shown in the complex ζ' plane for three specific values of k_1H; the other parameters are: $\rho_0 = 1.0$ g/cm³, $\rho_1 = 1.5$ g/cm³, $\rho_2 = 2.0$ g/cm³, $c_0 = 1540$ m/s, $c_1 = 1493.8$ m/s, and $c_2 = 1700$ m/s. It is clear that an increase in k_1H causes an increase in the number of poles which enter the first quadrant from the left and migrate to the right. Thus, leaky modes (Re$\zeta' < k_0/k_1$) may convert to trapped modes ($k_0/k_1 < \zeta' < 1$) and additional leaky modes may appear as k_1H increases.[33] For small changes in k_1H arising from frequency variations, the number of modes will not change, and we

expect that the relative contribution of the trapped modes will decrease with increasing frequency. This conclusion is based on the argument used to determine the source/receiver height dependence, where now we examine the behavior of the field for fixed source/receiver height and small changes in frequency. We then obtain Eq. (25) again, but the dependence on frequency is nonlinear because of the dispersive nature of the modes, i.e., $c_{r_1} = c_{r_1}(\omega)$. However, the expected decrease in the trapped mode contribution with an increase in frequency is evident in the example shown in Fig. 9.

In Figs. 10–12 we have plotted the relative contributions to the total field for the values of k_1H corresponding to the pole position plots in Fig. 8. In each case we have selected three combinations of f and H such that k_1H remains constant. As f increases and H decreases, the maximum range at which the trapped modes dominate becomes smaller. This is due to the decreasing contribution of the leaky mode field. Isolating the range dependence, we can write the leaky mode farfield as

$$p_2^{(L)} = \sum_n B_n e^{i\zeta_n r} = \sum_n B_n e^{ik_1\zeta'_n r},$$
$$= \sum_n B_n e^{-(\omega/c_1)\tau'_n r} e^{i(\omega/c_1)k'_{r_n} r}. \qquad (26)$$
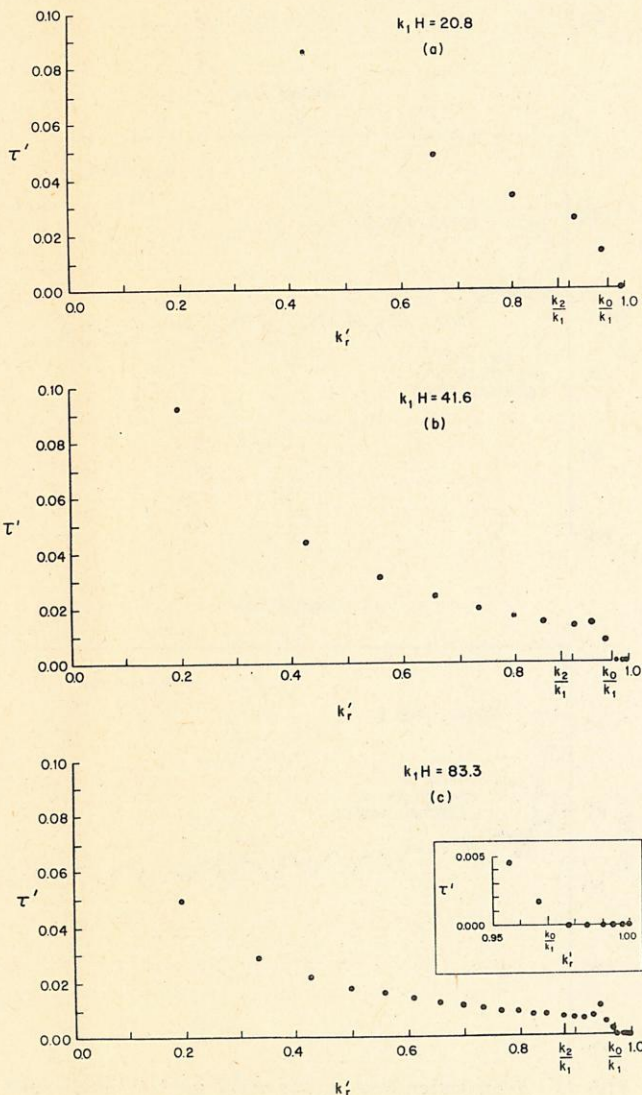
FIG. 8. Pole positions in the complex ζ' plane for 3% decrease in sound speed. (a) $k_1H = 20.8$, (b) $k_1H = 41.6$, (c) $k_1H = 83.3$.
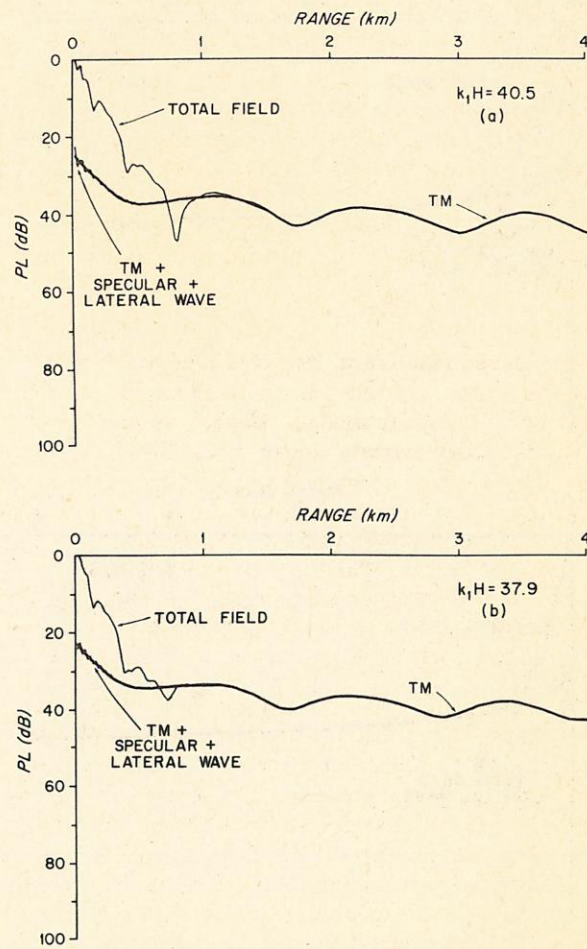
FIG. 9. Propagation loss vs range for small variations in k_1H: (a) $f = 107$ Hz, $k_1H = 40.5$, (b) $f = 100$ Hz, $k_1H = 37.9$. $H = 90$ m, $z + z_0 = 2$ m, 3% decrease in sound speed. Three trapped modes, nine leaky modes.

For fixed m_1, m_2, k_2/k_1, k_0/k_1, and $k_1 H$, the ζ_n' are fixed. Thus, the leaky mode fields at different frequencies but equal $k_1 H$ will be range-scaled versions of the same field. This result is not strictly true because of the frequency/dependence of the coefficients B_n. However, that dependence is weak, and the range-scaling is evident in Figs. 10–12.

Finally we shall present an example for which the sound speed in the layer is different from the previous cases. We select $c_1 = 1516.9$ m/s which corresponds to a 1.5% drop (rather than 3%) in the speed relative to the water sound speed. We consider in Fig. 13 two frequencies and layer thicknesses which yield values of $k_1 H$ equal to those presented in the earlier examples.
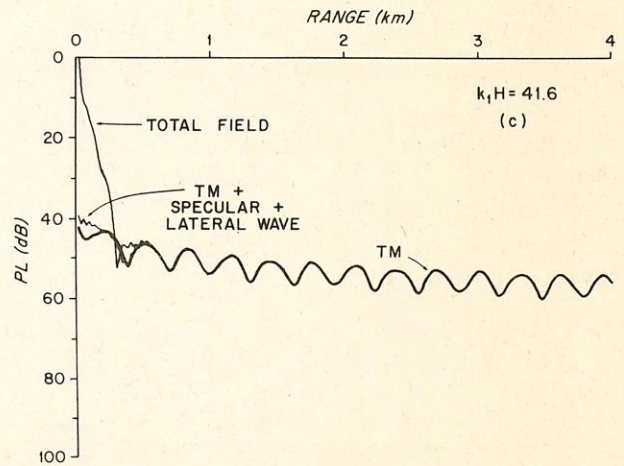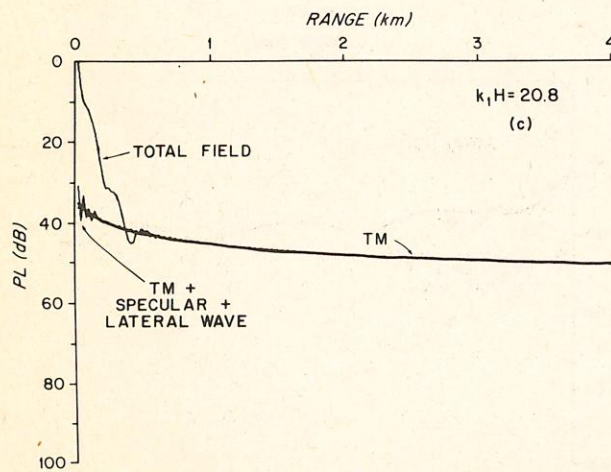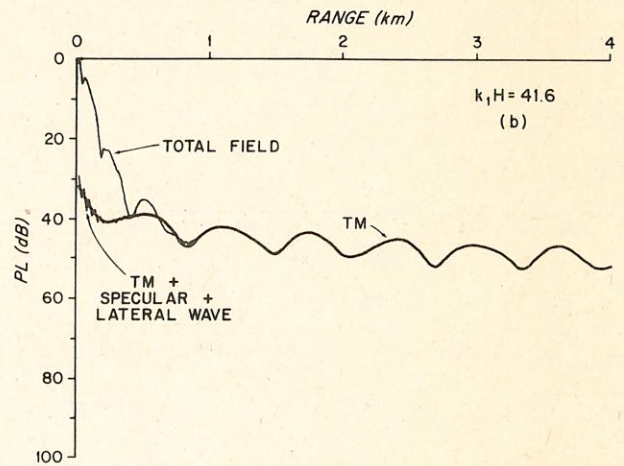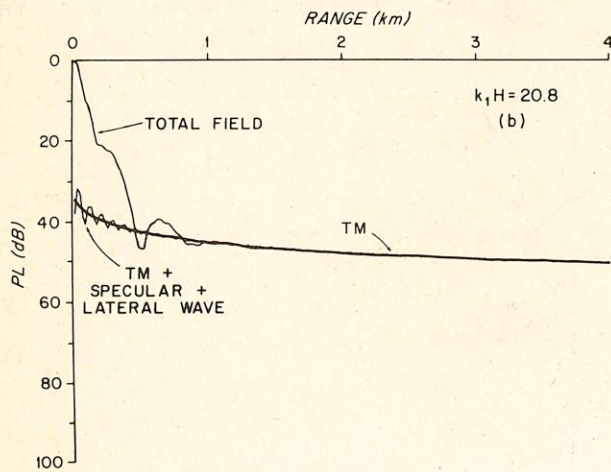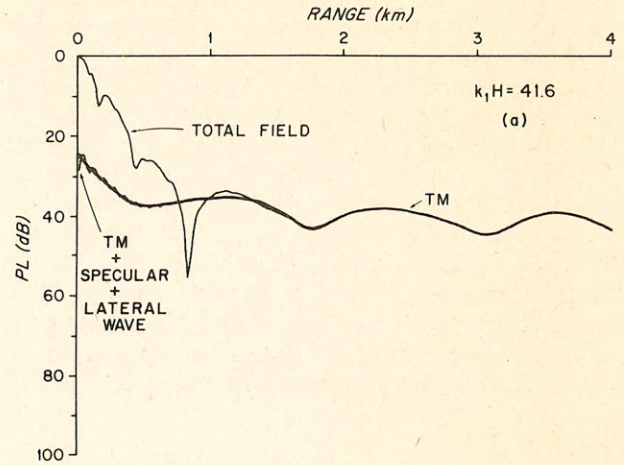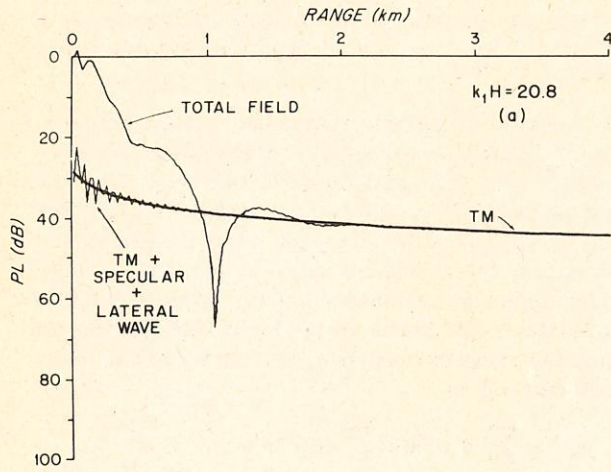
FIG. 10. Propagation loss versus range for $k_1 H = 20.8$: (a) $f = 55$ Hz, $H = 90$ m, (b) $f = 110$ Hz, $H = 45$ m, (c) $f = 220$ Hz, $H = 22.5$ m. $z + z_0 = 2$ m, 3% decrease in sound speed. One trapped mode, five leaky modes.

FIG. 11. Propagation loss versus range for $k_1 H = 41.6$: (a) $f = 110$ Hz, $H = 90$ m, (b) $f = 220$ Hz, $H = 45$ m, (c) $f = 440$ Hz, $H = 22.5$ m. $z + z_0 = 2$ m, 3% decrease in sound speed. Three trapped modes, ten leaky modes.

By comparison with Figs. 10 and 11, it is clear that the field is sensitive to small variations in c_1, even though k_1H and the other parameters are fixed.

III. CONCLUSION

We have examined the effects of normal modes in the bottom on the acoustic field in the ocean. In particular, we have focused attention on the perfectly trapped modes which are excited in a low-speed sediment layer by inhomogeneous waves emitted by a point source in the water column. Under certain circumstances, the effects of these modes may be significant.

The relative normal mode contribution to the total acoustic field in the water was calculated analytically for a near-bottom source/receiver geometry and evaluated for representative ocean bottom examples. It was found that, for combined source/receiver heights less than a wavelength, the field is dominated by the leaky mode contribution at short ranges ($\lesssim 2$ km) and the trapped mode contribution at long ranges ($\gtrsim 2$ km). For fixed bottom parameters, the trapped mode contribution increases exponentially with decreasing combined source/receiver height. Furthermore, it was found that for a fixed k_1H and c_1, the maximum range at which the leaky modes dominate decreases exponentially with increasing frequency. In fact, the leaky mode fields at different frequencies but equal k_1H are approximately exponentially range-scaled versions of the same field with a decay constant that is linearly proportional to frequency. Thus, we may conclude that resonances in the plane-wave reflection coefficient corresponding to the trapped modes are potentially measurable.

FIG. 12. Propagation loss vs range for $k_1H = 83.3$: (a) $f = 220$ Hz, $H = 90$ m, $(z + z_0)/\lambda_0 = 0.29$, (b) $f = 440$ Hz, $H = 45$ m, (c) $f = 880$ Hz, $H = 22.5$ m. $z + z_0 = 2$ m, 3% decrease in sound speed. Six trapped modes, 20 leaky modes.
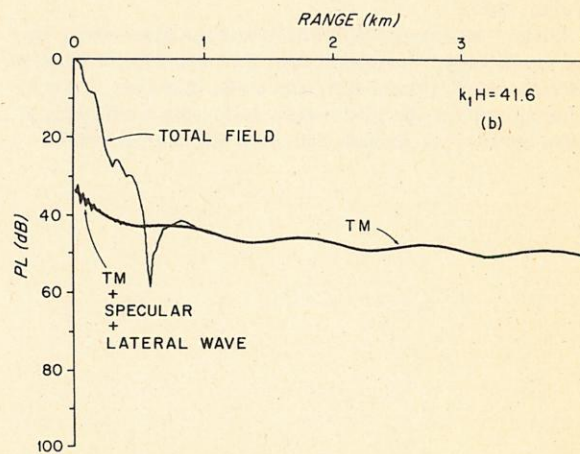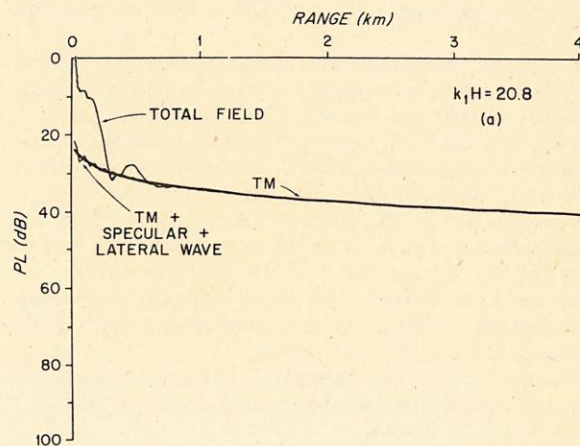
FIG. 13. Propagation loss versus range for 1.5% decrease in sound speed: (a) $k_1H = 20.8$, $f = 110$ Hz, one trapped mode, five leaky modes, (b) $k_1H = 41.6$, $f = 220$ Hz, two trapped modes, 11 leaky modes. $H = 45.7$ m, $z + z_0 = 2$ m.

Throughout this paper, attenuation in the bottom has been omitted for simplicity. It is expected that it would diminish the leaky mode and enhance the trapped mode contributions still further. Since the leaky modes propagate at steeper angles with correspondingly longer path lengths in the sediment layer, we would expect them to be more severely attenuated than the trapped modes. The effects of attenuation and sound speed gradients in the sediment are currently being investigated.

ACKNOWLEDGMENTS

[1] E. L. Hamilton, "Sound channels in surficial marine sediments," J. Acoust. Soc. Am. **48**, 1296–1298 (1970).

[2] E. L. Hamilton, "Geoacoustic models of the sea floor," in *Physics of Sound in Marine Sediments*, edited by L. Hampton (Plenum, New York, 1974).

[3] H. Lamb, *Hydrodynamics* (Dover, New York, 1932), 6th ed.

[4] F. Press and M. Ewing, "Theory of air-coupled flexural waves," J. Appl. Phys. **22**, 892–899 (1951).

[5] W. S. Jardetzky and F. Press, "Rayleigh wave coupling to atmospheric compression waves," Bull. Seism. Soc. Am. **42**, 135–144 (1952).

[6] F. M. Labianca, "Normal modes, virtual modes, and alternative representations in the theory of surface duct sound propagation," J. Acoust. Soc. Am. **53**, 1137–1147 (1973).

[7] M. A. Pedersen and D. F. Gordon, "Normal-mode theory applied to short-range propagation in an underwater acoustic surface duct," J. Acoust. Soc. Am. **34**, 105–118 (1965).

[8] M. A. Pedersen and D. F. Gordon, "Theoretical investigation of a double family of normal modes in an underwater acoustic surface duct," J. Acoust. Soc. Am. **47**, 304–326 (1970).

[9] T. Tamir and L. B. Felsen, "On lateral waves in slab configurations and their relation to other wave types," IEEE Trans. Ant. Propag. **AP-13**, 410–422 (1965).

[10] R. Fiorito and H. Überall, "Resonance theory of acoustic reflection and transmission through a fluid layer," J. Acoust. Soc. Am. **65**, 9–14 (1979).

[11] L. M. Brekhovskikh, *Waves in Layered Media* (Academic, New York, 1960).

[12] G. V. Frisk, "Inhomogeneous waves and the plane-wave reflection coefficient," J. Acoust. Soc. Am. **66**, 219–234 (1979).

[13] G. V. Frisk, A. V. Oppenheim, and D. R. Martinez, "Technique for measuring the plane-wave reflection coefficient of the ocean bottom," J. Acoust. Soc. Am. **62**, S66(A) (1977).

[14] A. V. Oppenheim, G. V. Frisk, and D. R. Martinez, "An algorithm for the numerical evaluation of the Hankel Transform," Proc. IEEE **66**, 264–265 (1978).

[15] A. V. Oppenheim, G. V. Frisk, and D. R. Martinez, "A Technique for the Evaluation of Circularly Symmetric Two-dimensional Fourier Transforms and its Application to the Measurement of Ocean Bottom Reflection Coefficients," in *Digital Signal Processing*, edited by V. Cappellini and A. G. Constantinides (Academic, New York, 1980).

[16] G. V. Frisk, A. V. Oppenheim, and D. R. Martinez, "A technique for measuring the plane-wave reflection coefficient of the ocean bottom," J. Acoust. Soc. Am. **68**, 602–612 (1980).

[17] A. V. Oppenheim, G. V. Frisk, and D. R. Martinez, "Computation of the Hankel transform using projections," J. Acoust. Soc. Am. **68**, 523–529 (1980).

[18] W. M. Ewing, W. S. Jardetzky, and F. Press, *Elastic Waves in Layered Media* (McGraw-Hill, New York, 1957).

[19] M. Abramowitz and I. A. Stegun, *Handbook of Mathematical Functions* (Natl. Bur. Stand. Appl. Math. Ser. **55**, Washington, DC, 1964).

[20] For details on complex analysis see e.g., R. V. Churchill, *Complex Variables and Applications* (McGraw-Hill, New York, 1960), 2nd ed.

[21] Reference 18, p. 59.

[22] I. S. Gradshteyn and I. M. Ryzhik, *Tables of Integrals, Series and Products* (Academic, New York, 1965).

[23] C. B. Officer, *Introduction to the Theory of Sound Transmission* (McGraw-Hill, New York, 1958), p. 113.

[24] Reference 18, p. 104.

[25] C. B. Officer, "The refraction arrival in water covered areas," Geophysics **18**, 805–810 (1953).

[26] K. Sezawa, "Love waves generated from a source of a certain depth," Bull. Earthquake Res. Inst. (Tokyo) **13**, 1–17 (1935).

[27] C. L. Pekeris, "Theory of propagation of explosive sound in shallow water," Geol. Soc. Am. Mem. **27**, Sec. 2, 1–117 (1948).

[28] Reference 11, pp. 350–353.

[29] Reference 18, p. 184.

[30] Reference 23, pp. 227–228.

[31] Reference 11, pp. 238–242.

[32] Large-scale versions of the plots can be obtained from G. V. Frisk.

[33] We note that with increasing k_r' (decreasing mode number), the dimensionless modal attenuation τ' does not decrease monotonically but increases and exhibits a local maximum for certain modes in the region $k_2/k_1 < k_r' < k_0/k_1$. This peak occurs for modes whose eigenangles are close to the Brewster (intromission) angle of zero reflection for a plane wave incident from medium 1 to medium 0 (for our case $k_r' = 0.945$ at the Brewster angle). These modes suffer the greatest transmission loss at the sediment–water interface and therefore exhibit a corresponding peak in modal attenuation.

MANDATORY DISTRIBUTION LIST

FOR UNCLASSIFIED TECHNICAL REPORTS, REPRINTS, AND FINAL REPORTS
PUBLISHED BY OCEANOGRAPHIC CONTRACTORS
OF THE OCEAN SCIENCE AND TECHNOLOGY DIVISION
OF THE OFFICE OF NAVAL RESEARCH

(REVISED NOVEMBER 1978)

1   Deputy Under Secretary of Defense
(Research and Advanced Technology)
Military Assistant for Environmental Science
Room 3D129
Washington, D.C. 20301

Office of Naval Research
800 North Quincy Street
Arlington, VA 22217
3   ATTN: Code 483
1   ATTN: Code 460
2   ATTN: 102B

1   CDR J. C. Harlett, (USN)
ONR Representative
Woods Hole Oceanographic Inst.
Woods Hole, MA 02543

Commanding Officer
Naval Research Laboratory
Washington, D.C. 20375
6   ATTN: Library, Code 2627

12   Defense Documentation Center
Cameron Station
Alexandria, VA 22314
ATTN: DCA

Commander
Naval Oceanographic Office
NSTL Station
Bay St. Louis, MS 39522
1   ATTN: Code 8100
1   ATTN: Code 6000
1   ATTN: Code 3300

1   NODC/NOAA
Code D781
Wisconsin Avenue, N.W.
Washington, D.C. 20235

SECURITY CLASSIFICATION OF THIS PAGE *(When Data Entered)*

REPORT DOCUMENTATION PAGE		READ INSTRUCTIONS BEFORE COMPLETING FORM
1. REPORT NUMBER WHOI-81-21	2. GOVT ACCESSION NO.	3. RECIPIENT'S CATALOG NUMBER
4. TITLE *(and Subtitle)* THE CONTRIBUTION OF NORMAL MODES IN THE BOTTOM TO THE ACOUSTIC FIELD IN THE OCEAN		5. TYPE OF REPORT & PERIOD COVERED Technical
		6. PERFORMING ORG. REPORT NUMBER WHOI Cont. #4507
7. AUTHOR(s) Mark K. Macpherson and George V. Frisk		8. CONTRACT OR GRANT NUMBER(s) N00014-77-C-0196
9. PERFORMING ORGANIZATION NAME AND ADDRESS Woods Hole Oceanographic Institution Woods Hole, Massachusetts 02543		10. PROGRAM ELEMENT, PROJECT, TASK AREA & WORK UNIT NUMBERS
11. CONTROLLING OFFICE NAME AND ADDRESS NORDA/National Space Technology Laboratory Bay St. Louis, MS 39529		12. REPORT DATE April 1981
		13. NUMBER OF PAGES
14. MONITORING AGENCY NAME & ADDRESS*(If different from Controlling Office)*		15. SECURITY CLASS. *(of this report)* Unclassified
		15a. DECLASSIFICATION/DOWNGRADING SCHEDULE

16. DISTRIBUTION STATEMENT *(of this Report)*

Approved for public release; distribution unlimited.

17. DISTRIBUTION STATEMENT *(of the abstract entered in Block 20, if different from Report)*

18. SUPPLEMENTARY NOTES

Reprinted from: J. Acoust. Soc. Am. 68 (2): 602-612. (August 1980).

19. KEY WORDS *(Continue on reverse side if necessary and identify by block number)*

1. Normal modes
2. Ocean bottom acoustics
3. Inhomogeneous waves

20. ABSTRACT *(Continue on reverse side if necessary and identify by block number)*

See reverse side.

DD FORM 1473 1 JAN 73   EDITION OF 1 NOV 65 IS OBSOLETE
S/N 0102-014-6601 |

The effects of normal modes in the bottom on the acoustic field in the ocean are examined. The ocean bottom model consists of a slow isovelocity half-space to simulate the characteristic sound velocity drop at the water-bottom interface. Attention is focused on the perfectly trapped modes which are excited in the layer by inhomogeneous waves emitted by a point source in the water column. The relative normal mode contribution to the total acoustic field in the water is calculated analytically for a near-bottom source/receiver geometry and evaluated for representative ocean bottom examples. It is shown that, for combined source/receiver heights less than a wavelength, the field is dominated by the leaky mode contribution at short ranges ($\lesssim$2km). and the trapped mode contribution at long ranges ($\gtrsim$ km). For fixed bottom parameter, the trapped mode contribution increases exponentially with decreasing combined source/receiver height. It is also shown that, for a fixed layer wavenumber-thickness product and fixed layer sound speed, the leaky mode fields at different frequencies are approximatley range-scaled versions of the same field.

Woods Hole Oceanographic Institution
WHOI-81-21

THE CONTRIBUTION OF NORMAL MODES IN THE BOTTOM
TO THE ACOUSTIC FIELD IN THE OCEAN by Mark K. Macpherson
and George V. Frisk. April 1981. Prepared for the
Office of Naval Research under Contract N00014-77-C-
0196.

The effects of normal modes in the bottom on the acoustic
field in the ocean are examined. The ocean bottom model con-
sists of a slow isovelocity half-space to simulate the charac-
teristic sound velocity drop at the water-bottom interface.
Attention is focused on the perfectly trapped modes which are
excited in the layer by inhomogeneous waves emitted by a point
source in the water column. The relative normal mode contri-
bution to the total acoustic field in the water is calculated
analytically for a near-bottom source/receiver geometry and
evaluated for representative ocean bottom examples. It is
shown that, for combined source/receiver heights less than a
wavelength, the field is dominated by the leaky mode contri-
bution at short ranges ($\gtrsim 2$ km) and the trapped mode contri-
bution at long ranges ($\gtrsim 2$ km). For fixed bottom parameter,
the trapped mode contribution increases exponentially with
decreasing combined source/receiver height. It is also shown
that, for a fixed layer wavenumber-thickness product and fixed
layer sound spe d, the leaky mode fields at different frequen-
cies are approximately range-scaled versions of the same
field.

1. Normal modes
2. Ocean bottom acoustics
3. Inhomogeneous waves
I. Macpherson, Mark K.
II. Frisk, George V.
III. N00014-77-C-0196

This card is UNCLASSIFIED